Thermally drawn fibers as nerve guidance scaffolds

Thermally Drawn Fibers as Nerve Guidance Scaffolds

Authors:
Ryan A. Koppes[12], Seongjun Park[1,3], Tiffany Hood[4], Xiaoting Jia[1], Negin Abdolrahim Poorheravi[5], Anilkumar Harapanahalli Achyuta[6], Yoel Fink[1,7], Polina Anikeeva[1,7]

Affiliations:
[1]Research Laboratory of Electronics, Massachusetts Institute of Technology, Cambridge, Massachusetts 02139
[2]Department of Chemical Engineering, Northeastern University, Boston, Massachusetts 02115
[3]Department of Electrical Engineering and Computer Science, Massachusetts Institute of Technology, Cambridge, Massachusetts 02139
[4]Department of Bioengineering, Massachusetts Institute of Technology, Cambridge, Massachusetts 02139
[5]Department of Mechanical Engineering, Massachusetts Institute of Technology, Cambridge, Massachusetts 02139, United States
[6]Draper Laboratory**,** 555 Technology Square, Cambridge, Massachusetts 02139
[7]Department of Materials Science and Engineering, Massachusetts Institute of Technology, Cambridge, Massachusetts 02139

Corresponding Author:

Polina Anikeeva, Ph.D.

Mailing Address: 77 Massachusetts Ave, 8-425
Cambridge, MA 02139

Phone: 617-253-3301
anikeeva@mit.edu

Abstract (100-200 Words):

Synthetic neural scaffolds hold promise to eventually replace nerve autografts for tissue repair following peripheral nerve injury. Despite substantial evidence for the influence of scaffold geometry and dimensions on the rate of axonal growth, systematic evaluation of these parameters remains a challenge due to limitations in materials processing. We have employed fiber drawing to engineer a wide spectrum of polymer-based neural scaffolds with varied geometries and core sizes. Using isolated whole dorsal root ganglia as an *in vitro* model system we have identified key features enhancing nerve growth within these fiber scaffolds. Our approach enabled straightforward integration of microscopic topography at the scale of nerve fascicles within the scaffold cores, which led to accelerated Schwann cell migration, as well as neurite growth and alignment. Our findings indicate that fiber drawing provides a scalable and versatile strategy for producing nerve guidance channels capable of controlling direction and accelerating the rate of axonal growth.

Key Words: Peripheral Nerve Repair, Neural Scaffold, Fiber Drawing, Tissue Engineering

1. Introduction

Injuries to the peripheral nervous system (PNS) affect a broad population globally and often result in life-long disabilities in 60% of the patients due to the limited regenerative ability of neural tissue [1]. Following PNS injury, regenerating axons from the proximal nerve stump have to span the injury site and reconnect with the distal targets. While spontaneous recovery can occur for small-gap injuries (less than 2 cm), regeneration across larger injuries is impeded by a combination of factors including immune response, scarring, poor support cell repopulation, and neuronal death [2, 3]. The common PNS surgical intervention for small-gap injuries, fascicular neurorrhaphy that sutures the ends of the proximal and distal nerve stumps together, adequately restores function only in ~50% of patients [4]. Autografting of the donor tissue is commonly used for injuries greater than 2 cm [5]. While ubiquitous in clinic, this method is limited by the availability of donor tissue, and poses a risk of secondary co-morbidity and neuroma formation [6, 7]. For complete nerve transections with gap distances greater than 4 cm, functional recovery becomes highly unlikely even with surgical intervention [8].

Nerve guidance scaffolds promoting axonal growth may in future provide therapeutic alternatives to autografts. While a variety of synthetic and biopolymers, such as collagen, polycaprolactone, polyglycolic acid, poly-DL-lactide-co-caprolactone (PLCL), and polyvinyl alcohol (PVA), [9] have been explored as scaffold materials, geometry of these devices remains largely limited to simple cylindrical lumens with millimeter dimensions [10-13]. Since individual fascicle dimensions are on the order of microns, which is ~1000 times smaller than typical scaffolds, the role of the channel size on Schwann cell migration and axonal growth remains poorly understood especially for channels smaller than 200 µm. To date, limited work on systematically investigating the effects of microchannel size and geometry on neurite growth has been carried out in polydimethylsiloxane (PDMS) [14] and alginate [15] gels. Furthermore, only a few scaffolds incorporating multiple channels have been reported [16, 17].

As the role of a synthetic scaffold is to accelerate nerve repair across the injury site, a number of strategies' have been explored to increase axonal growth within these devices. These include drug delivery [18], addition of cellular components [19, 20], electrical stimulation [21, 22], and topography [23]. The latter has been primarily studied in the context of flat lithographically patterned substrates [10, 23-25] limited to

macroscopic rolling for experiments *in vivo* [12]. Consequently, despite the abundance of literature illustrating the growth promoting effects of topographical features [10], nerve guidance channels approved for clinical use remain limited to a simple round geometry [26].

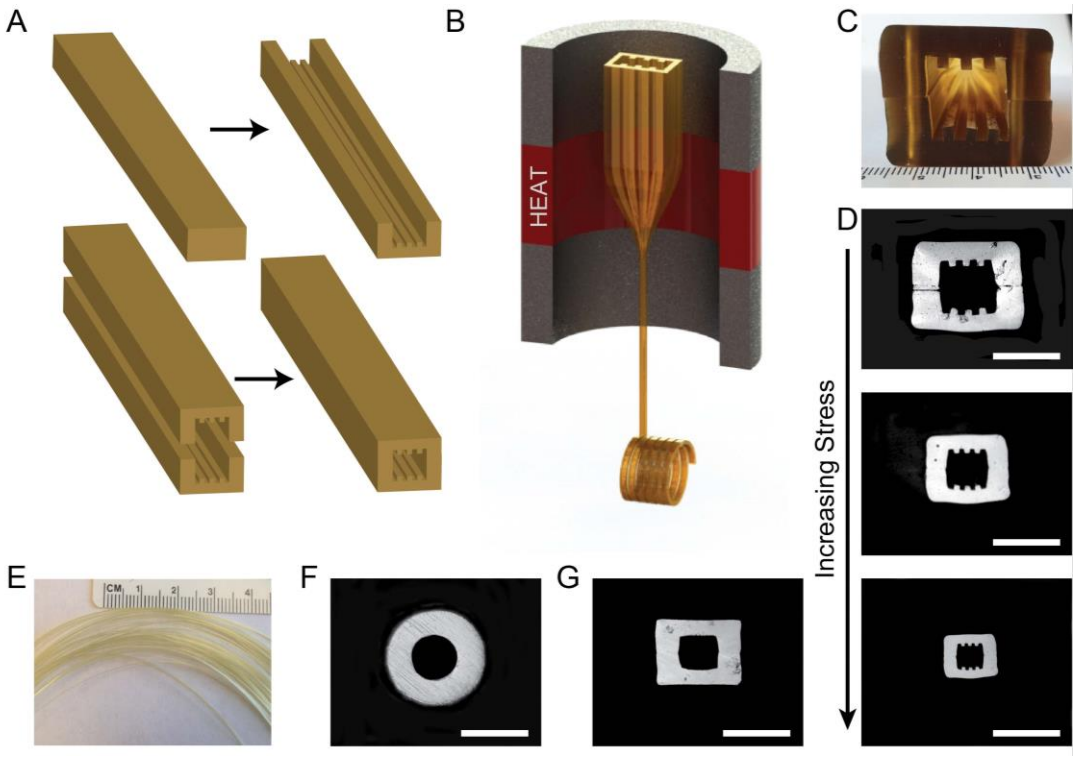

Fig. 1. The thermal drawing process and fiber cross-sections for neural guidance channels. (A) A macro scale preform was fabricated by first machining features into PEI slabs, consolidated, and (B) loaded within the draw tower and heated above the glass transition temperature. (C) Cross-section of machined preform prior to consolidation. (D) The draw down ratio is increased with increasing stress applied via the capstan, yielding a range of fiber dimensions and (E) hundreds of feet of micro scale fiber while maintaining the geometry of the original preform. Scaffolds were also made with (F) round and (G) square geometries. Scale bars = 200 μm

We hypothesize that the current materials processing techniques have been limiting the geometries of neural guidance channels and propose an alternative approach to fabrication of these devices. We employ thermal drawing process (TDP) [27, 28] commonly used in fiber photonics and recently applied to neural probe design [29, 30], to produce flexible, biocompatible polymer-based neural scaffolds with a variety of geometries and dimensions. The versatility of TDP enabled us to produce, with accuracy, an array of neural scaffolds with cylindrical and rectangular core geometries and dimensions approaching those of single fascicles (inner sizes 50-200 μm and lengths up to tens of centimeters). Furthermore, TDP allowed for direct integration of

Table 1 Mechanical Properties of Thermally Drawn NGCs. Properties were calculated for fibers of 10 mm in length and inner diameter/widths of 50 to 200 μm.

	k_{Axial} (N/m)	$k_{Bending}$ (N/m)
Round (50-200 μm)	213.9-3423.0	0.0011-0.2953
Square (50-200 μm)	33.9-1020.9	0.0002-0.2966

microgrooved topography within the structure of scaffold channels. The palette of fiber-based neural scaffolds allows for the first time, a detailed *in vitro* analysis of channel size, geometry, and surface topography for potentially promoting nerve regeneration.

2. Materials and Methods

2.1 NGC fabrication

Scaffold fibers were produced using the thermal drawing process (Fig. 1). Bulk polymer materials were annealed in a vacuum at 105°C for one month prior to fabrication. Macroscale polyetherimide (PEI, Tg = 216°C) slabs or cylinders were machined to include the desired channel geometries (round, square, or grooved). If needed, machined PEI slabs were consolidated in a pneumatic heated press at 240°C to form the final preform (Fig. 1A). Preforms were mounted onto a vertical draw tower, (Fig. 1B) and drawn at 325°C producing hundreds of meters of fiber. Increasing stress during fiber drawing allowed for tuning of channel dimensions from 300 μm to 40 μm.

2.2 Cross sectional imaging

Fiber scaffolds were sealed in an epoxy matrix and mechanically polished with a semiautomatic polisher/grinder (RotoPol-1, Struers). Cross sections of the fibers were then imaged using an optical microscope (Axioskop, Carl Zeiss Inc.) in transmission mode (Fig. 1).

2.3 Mechanical Properties

The axial spring constant for round and rectangular PEI fibers with an elastic modulus of 104.8 MPa and a fiber length of 10 mm (Supplementary Information) was calculated according to Kozai et al. [31].

2.4 Isolation of Dorsal Root Ganglia

All animal procedures were approved by the MIT Committee on Animal Care and carried out in accordance with the National Institutes of Health Guide for the Care and Use of Laboratory Animals. Primary dorsal root ganglia (DRGs) were isolated from Sprague Dawley neonatal rats postnatal day 1 (P1; Charles River) as previously reported [32]. The spinal cord was exposed and isolated using a posterior approach. Individual DRG explants were collected from the lumbar region, trimmed of nerve roots and connective tissue, and placed in Hibernate A media supplemented with B-27 and glutamax (Life Technologies) for up to 7 days at 4°C for use on-demand. On average, 10-15 DRGs were extracted from each animal and mixed.

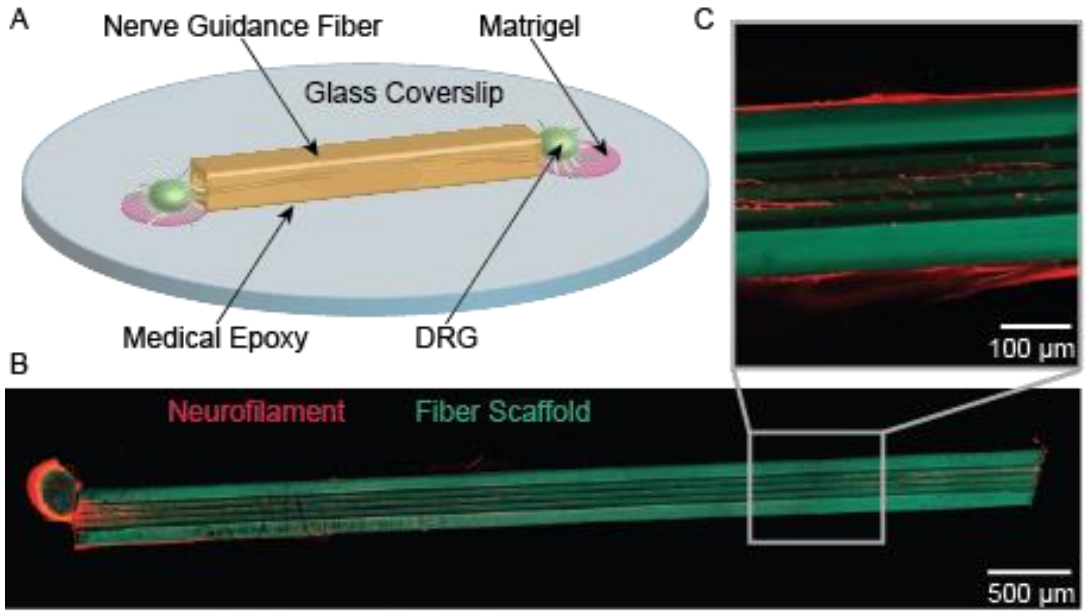

Fig. 2. (A) Schematic representation of a DRG seeded fiber-coverslip assembly. (B) Neurite ingrowth through a grooved, 5 mm fiber scaffold (red = neurofilament, cyan = fiber scaffold). (C) A higher magnification image of neurite orientation along the inner topographical features. Neurite outgrowth is observed both within and along the surface of the fiber scaffolds.

2.5 In vitro evaluation of fiber neural scaffolds

Fibers were first sectioned into desired lengths (5 or 10 mm). Sections were then affixed with medical epoxy (Loctite M-31CL) to 12-mm glass coverslips (Electron Microscopy Sciences). Prior to fiber attachment, coverslips were etched with 10% HCl solution (Sigma) and stored in 99% ethanol for use on demand. Coverslips were dried and placed into 24-well tissue culture plates (VWR Scientific Products). Fiber and coverslip assemblies were rinsed 3 times with 70% ethanol (EtOH) and subsequently incubated in

750 µl EtOH for 24 hrs. Assemblies were then rinsed 3 times with sterile water and left to dry in a biosafety cabinet. Once dry, coverslip assemblies were subjected to 15 minutes of UV sterilization. To aid initial DRG adhesion to coverslips, 2.5 µl drops of 1:30 dilution of reduced growth factor Matrigel™ (BD Biosciences) in growth media (Neurobasal-A medium supplemented with B-27, Glutamax (Life Technologies), 1% Penicilllin-Streptomycin (Lonza), 25 ng/mL 2.5S nerve growth factor (Life Technologies) were deposited onto glass at the longitudinal ends of each fiber. Matrigel™ drops were incubated (37° C, 5% CO_2) for 3 hours and following incubation, 500 µl of growth media was added to fiber assembly and incubated for 24 hours to allow the media to completely fill and flow freely through the fiber microchannels.

Whole DRG were manually seeded onto the Matrigel™-coated areas next to the fiber scaffolds at one or both ends of the fiber and incubated (Figs. 2 and 3) for 14 days. Growth media was exchanged every 3-5 days. Following growth, seeded fiber assemblies (n=6 per geometry, dimension, and seeding condition of a single DRG or a pair of DRGs for a total of 144 samples) were fixed in 4% solution of paraformaldehyde (Sigma) in phosphate buffered saline (PBS) for 45 minutes. Note, that for these experiments DRGs were picked at random from a mixture of DRGs extracted from 8-10 animals.

2.6 Immunocytochemistry

Fixed samples were rinsed 3 times with phosphate buffered saline (PBS) and permeabilized for 25 minutes with 0.1% Triton X-100 in PBS and then stained with antibodies against neurofilament and F-actin. Samples were blocked overnight at 4□C in 2.5% goat serum in PBS (GS), and then incubated for an hour at room temperature with 1:500 rabbit anti-neurofilament 200 (N4142, Sigma) and 1:500 mouse anti-S-100 (S2657, Sigma) primary antibodies diluted in GS. Following incubation with primary antibodies, samples were rinsed 3 times for five minutes with PBS and then incubated with 1:1000 Alexa Fluor® 488 Phalloidin (A12379, Life Technologies), 1:1000 goat anti-mouse Alexa Fluor® 568 IgG (A11004, Life Technologies), and 1:1000 goat-anti-rabbit Alexa Fluor® 633 IgG (A21070, Life Technologies) secondary antibodies at room temperature for an hour. All labeled samples were rinsed 3 times for 5 minutes in PBS prior to mounting on a glass slide with Prolong Gold Anti-fade containing 4', 6-diamidino-

2-phenylindol (DAPI; Life Technologies) to label all cell nuclei. Mounted slides were stored at –20□C prior to imaging.

2.7 Microscopy and Image Analysis

Fiber-DRG hybrid samples were imaged with an Olympus FV1000 laser scanning confocal microscope with a 10X dry objective to examine total neurite outgrowth. Full z-stacks through the fibers were collected at the edges with a 25X water immersion objective to evaluate morphological features of the DRG processes entering the channels (Supplementary Fig. 1). The collected images were analyzed for neurite length and growth direction (Supplementary Fig. 2) as well as orientation of nuclei (Fig. 5A and Supplementary Fig. 3), similarly to previously described [25, 26], in a custom-written software in Matlab® (Mathworks) with Image-Processing toolbox.

In all cases, images were converted to binary using Otsu's thresholding method. A single image from the z-stack was selected to analyze nuclear orientation (Supplementary Fig. 3). Shapes of nuclei were fit with ellipsoids (Fig. 5A) to find the major and minor axis. The nuclear aspect ratio (NAR) was defined as a ratio of the major to minor axis (NAR = length/width). Alignment was characterized as the difference between the angle of the major axis of the nucleus and the direction of the channel (normalized to 0°).

To evaluate neurite alignment within different fiber scaffold geometries, a two-dimensional maximum projection image was created from all of the corresponding z-stack images (Supplementary Fig. 1) and the binary backbone of neurofilament staining was inspected sequentially in 5×5 pixel boxes, and a major angle of positive pixels was found. For the entire neurofilament backbone, the major angles were binned across 180° at 2° increments (Supplementary Fig. 2). Bright pixels per bin were normalized to the total number of bight pixels to account for differences in the quantity of positive pixels across images. For each image, the resultant histogram curve was fit with a normalized Gaussian function:

$$f(\theta) = \frac{1}{\sigma\sqrt{2\pi}} e^{-(\theta-\phi)^2 / 2\sigma^2} \quad (5)$$

where θ is the angle with respect to the longitudinal axis of fiber, ϕ is the peak angle of alignment for neurite ingrowth, and σ is the standard deviation from that peak.

2.8 Statistical Analysis

Group size was determined by a power analysis in Matlab® with the Statistics toolbox, under the assumption that a grooved fiber geometry would increase the length of neurite growth as compared to round-channel control fibers (=0.05, power=0.9). Statistical significance was assessed by first ensuring normal distribution and comparable variance across the datasets via Lilliefors and Bartlett's tests, respectively, followed by an ANOVA and Tukey's post-hoc comparison test in Matlab®.

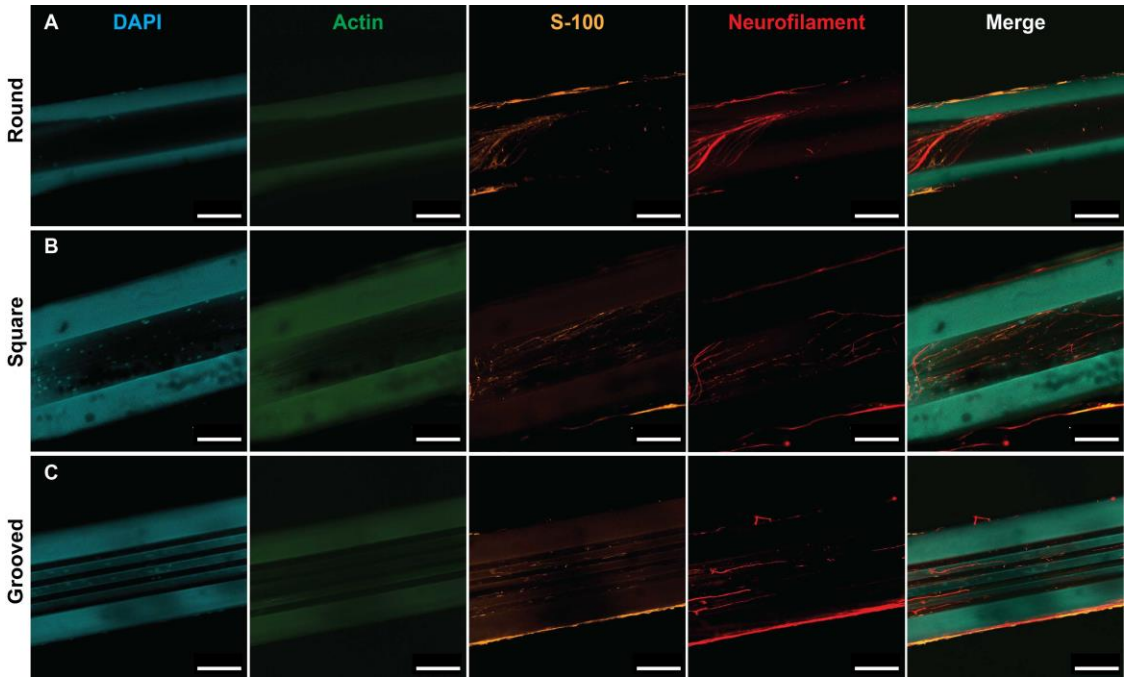

Fig. 3. DRG outgrowth into the lumen of fiber NGCs after fourteen days of growth. Fibers were fixed and stained for cell nuclei (DAPI, blue), F-actin (phallodin, green), Schwann cells (S-100, orange), and neurites (neurofilament, red). Growth into (A) round, (B) square, and (C) grooved NGCs. Substantial autofluorescence of PEI fibers can be observed in the blue and green channels. Scale bars=100 μm

3. Results

3.1 Thermally Drawn Fiber Scaffolds

The thermal drawing process is advantageous for three-dimensional integration of materials and miniaturizing features, otherwise difficult to achieve at scale with traditional microfabrication techniques. In this study we have focused on the role of scaffold geometry in supporting and accelerating neurite outgrowth *in vitro*. Hence we have

fabricated a broad palette of fiber scaffolds based on polyetherimide (PEI), which was found to support cell adhesion *in vitro* [33, 34] and exhibited high biocompatibility *in vivo* [29]. Fiber scaffolds with rectangular cores incorporating microgrooves (Fig. 1D), smooth round (Fig. 1F) and rectangular cores (Fig. 1G) were fabricated across a wide range of channel dimensions (Fig. 1D). Hundreds of meters of fiber (Fig. 1E) with core dimensions systematically varied between 40 μm and 200 μm were produced from individual templates, preforms, by controlling drawing speed and temperature. The sharp corners of rectangular microchannels and integrated grooves were well preserved during the drawing (Fig. 1). Fiber scaffolds are axially stable, but have an inherently low flexural spring constant, bending easily while maintaining their geometry and functions (Table 1).

3.2 Ingrowth of Dorsal Root Ganglia Neurites into Fiber Scaffolds

We have investigated neurite outgrowth within PEI-based fiber scaffolds with round, rectangular, and grooved cores with inner dimensions of 50, 100, 150 and 200 μm and lengths of 5 mm or 10 mm. To mimic a gap in peripheral nerve tissue, single DRGs and DRG pairs were seeded on the longitudinal ends of the fiber scaffolds mounted on cover glass substrates (Fig. 2). For all cases, outgrowth was observed on the substrate, along the fiber interface, on the surface of the fiber scaffolds, and within their micro channels (Fig. 3). The majority (92.3%) of cell bodies located within the microchannels stained positive for S-100, indicating the migration of Schwann cells into fiber scaffolds (Fig. 3).

For 5 mm long fiber scaffolds, the length of neurite outgrowth into the channel is significantly ($p<0.05$) higher for grooved and rectangular channels as compared to a simple round geometry for the single and paired DRG experiments (Fig. 4A-B). For grooved fiber scaffolds neurite outgrowth for single and paired DRGs extends through the entire length of the channel regardless of the core dimensions. In contrast, for 5 mm long round-channel fibers seeded with single DRGs, neurite outgrowth is 1.9 fold greater in 50 μm channels than in 200 μm channels (Fig. 4A). Averaged across all dimensions (50-200 μm), neurite length in the single DRG experiments is 2.4 times and 3.4 times greater for rectangular and grooved channels, respectively, as compared to round cores (Fig. 4A). In experiments involving a pair of DRGs seeded at the opposing edges of the fibers, the total length of growth into all channels is increased for all core geometries, and appears independent of dimensions with the exception of a 1.1 fold increase for 50 μm vs 200 μm rectangular scaffolds (Fig. 4B). Consistent with single-DRG experiments,

averaged across all dimensions, neurite growth is 1.8 and 1.9 fold greater for rectangular and grooved channels as compared to a round geometry (Fig. 4B).

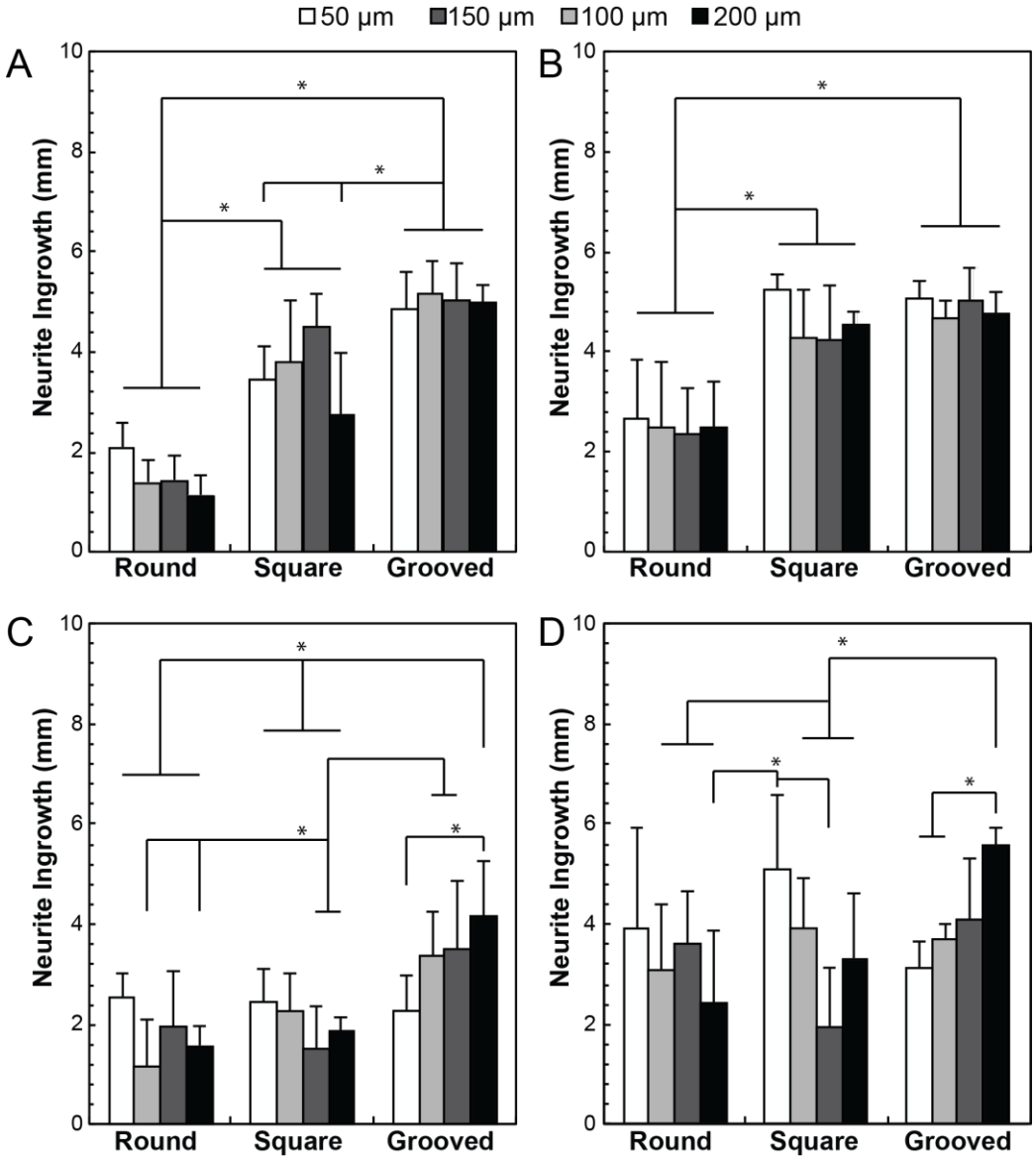

Fig. 4. Average DRG ingrowth into the lumen of fiber NGCs after fourteen days of growth for round, square, and grooved of (A, B) 5 mm and (C, D) 10 mm NGCs. Both lengths of NGCs were seeded with a DRG at (A, C) one end or (B, D) both ends. All values are mean ± S.D. *Statistically significant ($p<0.05$) (one-way ANOVA)

For 10-mm long fiber scaffolds seeded with single DRGs, averaging across all channel dimensions shows a 1.1 and 1.8 fold increase in neurite growth for rectangular and grooved channels over the round geometry (Fig. 4C). Furthermore, for round channel fibers, a 1.6 fold increase in neurite outgrowth is observed for 50 µm channels as compared to 200-µm channels. In contrast, for grooved fibers a 1.9 fold neurite

outgrowth increase is observed for larger, 200-μm fibers as compared to narrower 50-μm fibers (Fig. 4C). When two DRGs are seeded at both ends of fiber scaffolds, these trends diminish across all geometries, with the exception of a 1.8 increase observed for neurites growing within grooved 200-μm fibers as compared to 50-μm scaffolds (Fig. 4D).

3.3 Nuclear Aspect Ratio and Alignment within Fiber Scaffolds

Fiber geometry and dimensions strongly influenced the orientation of cell nuclei within the scaffold channels. The alignment of the nuclei with respect to the scaffold was quantified via the nuclear aspect ratio (NAR), the ratio of the major to minor axis of the ellipsoids fitted to nuclei, and the angle between the major axis and the scaffold axis of symmetry. Across all dimensions, the nuclear angles were 1.6 times smaller for scaffolds with grooved channels as compared to round channels, indicating greater alignment afforded by integrated topography (Fig. 5B). In rectangular channel fibers, dimensions have the largest influence on nuclear alignment as indicated by 4.8 fold decrease in nuclear angle for 50-μm core as compared to 200-μm core fibers (Fig. 5B). NAR that has been previously correlated with cell migration [35], was substantially influenced by channel dimensions for both round and rectangular channel geometries. A difference in NAR of 2.5 and 2.4 fold was observed between 50 μm and 200 μm-core fibers for round

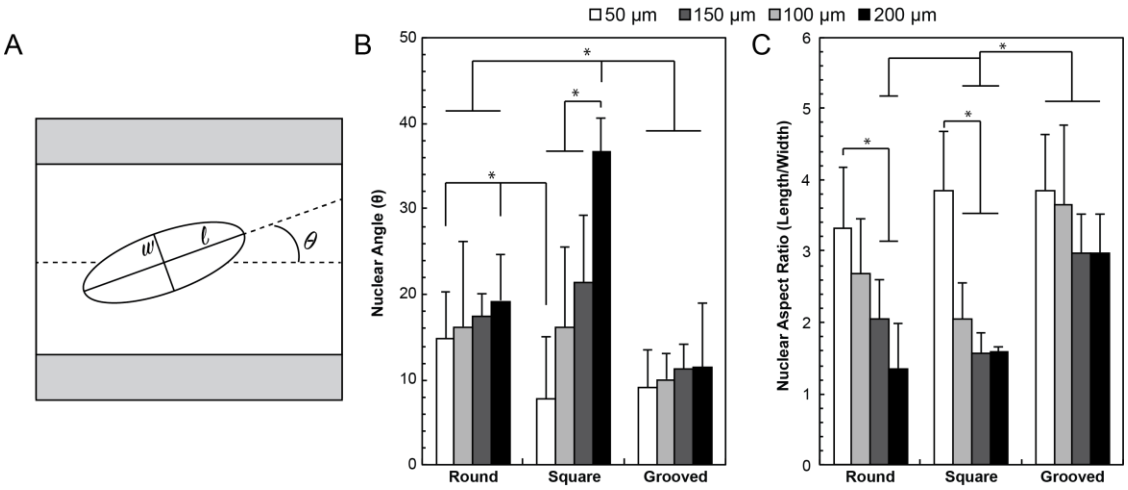

Fig. 5. Cell nuclei orientation and aspect ratio were found for all fiber geometries and dimensions as indication of cell migration and alignment along the length of the channel. (A) Nuclei were fit with an ellipse to find the major (*l*) and minor (*w*) diameters to calculate nuclear aspect ratio as well as the angle between the major axis and the angle of the channel. (B) Cell nuclei were more aligned along the length of the channel for narrower round and square fibers (50 μm compared to 200 μm), but demonstrated a high degree of alignment for all dimensions of grooved NGCs. (C) A higher nuclear aspect ratio was observed for narrower round and square channels as well as all grooved NGCs. All values are mean ± S.D. *Statistically significant ($p<0.05$) (one-way ANOVA)

and rectangular geometries, respectively (Fig. 5C). In contrast, grooved channels maintained a high NAR (3.4 average) across all dimensions (Fig. 5C).

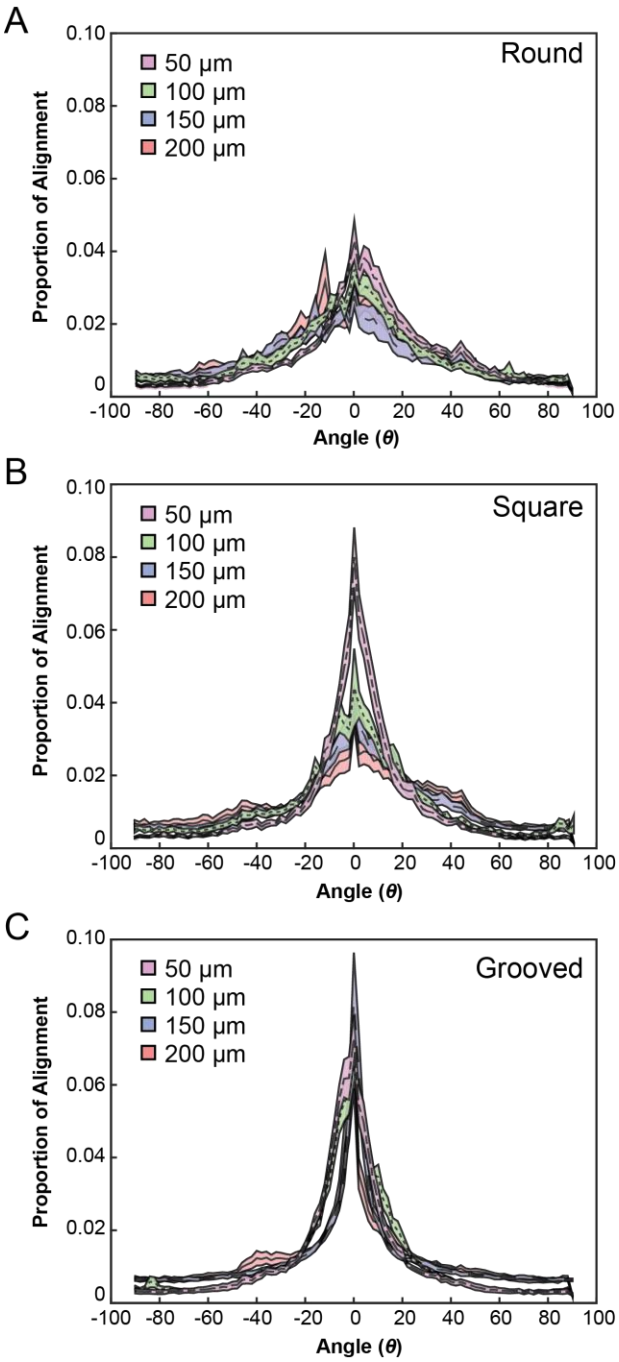

Fig. 6. Neurite ingrowth is more aligned along the length of narrower and grooved NGCs. Histogram average traces ± S.E. for neurite orientation angle for (A) round, (B) square, and (C) grooved NGC geometries and dimensions (50, 100, 150, 200 µm).

3.4 Influence of Channel Geometry and Dimensions on Neurite Alignment

Geometric constraints promote neurite alignment within the channel as evident from the comparison between the DRGs growing into narrower vs. wider channels (Fig. 6). Peak angles (ϕ) and angular deviations (σ) with respect to the scaffold axis of symmetry were found by applying a normalized Gaussian fit to the distribution of binned angles for each fiber geometry and dimension. The influence of the channel width is most apparent in the square geometry (Fig. 6B) with a 2.4 fold decrease in the deviation observed for 50-µm core fibers as compared to 200-µm core devices. The inclusion of topography within fiber channels resulted in sharp rectification of the dispersion of neurite alignment (Fig. 6C, Table 2).

3.5 Correlation of Orientation Parameters and Neurite Outgrowth

A negative correlation between NAR and neurite orientation was found, which indicated that nuclei with larger NARs are accompanied by greater confinement of the neurite outgrowth along the direction (axis of symmetry)

of the channel (Fig. 7A). Similarly, the higher degree of alignment of nuclei along the channel (smaller nuclear angle) is positively correlated to a higher degree of alignment of neurites through the channel (Fig. 7B).

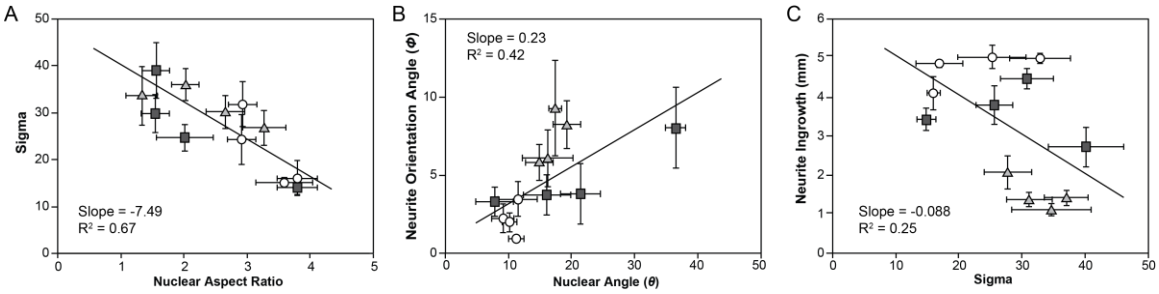

Fig. 7. Correlation scatter plots for neurite alignment fits, nuclear aspect ratio, and neurite ingrowth. (A) A negative correlation exists between NAR and the deviation of neurite alignment. (B) The angle of neurite alignment and nuclei alignment are positively linked. (C) For 5-mm fibers seeded with one DRG, neurite outgrowth is slightly negatively correlated to the deviation of neurite alignment. This trend may be masked by the square and grooved NGCs' neurite growth saturated.

4. Discussion

The thermal drawing process affords high throughput fabrication of neural scaffolds, while allowing for fine control over channel geometries and dimensions (Fig. 1). Microscopic features of fiber-based scaffolds are defined on the macroscale without the need for advanced materials processing techniques such as lithography or

Table 2 Gaussian fit parameters for neurite orientation. All values are mean ± S.D.

	50-μm	100-μm	150-μm	200-μm
Mean (*μ*)				
Round	5.8±2.8	0.2±7.6	-7.6±9.4	-3.2±8.6
Square	1.4±3.8*	0.4±4.9	2.1±5.8	1.2±10.3
Grooved	-2.1±2.3*	0.1±2.	0.1±1.0	-1.4±4.3
Variance (*σ*)				
Round	5.8±2.8	6.1±7.6	9.4±7.6	8.3±3.8#
Square	3.3±2.4*	3.8±3.2	3.8±4.8	8.1±6.4#
Grooved	2.2±2.2*	2.0±1.5	0.9±0.4*	3.5±2.8*

* Statistically significant from Round fiber of same dimension ($p<0.05$; one-way ANOVA)
# Statistically significant from 50-μm of same geometry ($p<0.05$; one-way ANOVA)

electrospinning. Multiple drawing steps can be implemented to produce scaffolds with multiple channels and/or channels with dimensions well below 50 μm [29] enabling unprecedented control over scaffold geometry for neural tissue engineering.

Taking advantage of the drawing process to rapidly produce a broad palette of fiber scaffolds with varied channel geometries and dimensions spanning 50-200 μm, we investigated the role of scaffold structure on neurite growth from isolated DRGs *in vitro*. In agreement with previous reports [10], we found that microgrooves or topographical features enhance neurite growth within the reported fiber scaffolds (Fig. 4). Fiber geometry appeared as a predominant factor influencing neurite outgrowth (Fig. 4, 7), and introduction of sharp corners and microgrooves yielded longer processes. For fibers with round and rectangular cross sections, however, narrower channels led to an enhanced neurite growth (Fig. 4). Channels with dimensions <40 μm were less likely to host growing neurites (Supplementary Figure 4), with an average ingrowth of <150 μm observed for 30 fibers 5-10 mm long.

Increased ingrowth was accompanied by greater NAR (Fig. 5) and increased nuclear (Fig. 5) and neurite orientation (Fig. 6) within fiber scaffolds. The potential geometric and dimensional similarity of the narrower scaffolds to individual nerve fascicles may underlie the alignment of neurites along the channel direction resulting in the observed enhanced outgrowth (Fig. 7). Consequently, in future applications *in vivo*, fiber scaffolds integrating multiple smaller channels may provide biomimetic substitutes to autografts.

The introduction of topographic features into scaffold channels effectively decoupled neurite alignment and outgrowth from the channel size, as similar trends were found across all dimensions. Previous *in vitro* and *in vivo* studies have shown that growing axons are influenced by topographical cues [10] such as electrospun fibers [19, 36-41], microgrooves [11, 37] or dense nanowire arrays [42]. For the fiber scaffolds reported here, topography appears to rectify neurite and cellular alignment even in larger channels (Fig. 3 and 4) while also allowing for robust ingrowth into the channel. Additionally, the fibers themselves act as guidance cues for neurite outgrowth with substantial growth observed on the surface of fibers with both rectangular and round external cross sections (Supplementary Fig. 5) or within large square-channel fibers without the addition of Matrigel® to the glass substrates (Supplementary Fig. 6).

As PNS repair is highly dependent upon the supportive behavior of Schwann cells [43-45], understanding glial migration may provide insights into overcoming growth-inhibiting responses to nerve injury [35]. Since the topography of Schwann cells can influence the

orientation of neurite outgrowth, we investigated the migration of these cells within the fiber scaffolds. Consistent with migration of glia [35, 46], the observed alignment and increased NAR of the Schwann cell nuclei within the scaffold channels is correlated with the neurite growth and alignment (Fig. 7). In agreement with previous studies, we find that Schwann cell migration is accelerated by the presentation of microgrooves (Fig. 5) [47, 48].

Table 3 Neurite outgrowth from a single DRG on the surface and edges of 10 mm NGC fibers. All values are mean ± S.D.

	50-µm (mm)	100-µm (mm)	150-µm (mm)	200-µm (mm)
Round	5.7±0.7	5.9±1.4	4.9±0.8	4.7±1.1
Square	5.4±0.9	4.9±0.7	4.6±1.1	4.9±1.2
Grooved	5.5±0.9	5.5±1.0	5.5±1.1	5.2±0.9

While this study employed PEI as a biocompatible platform for scaffold fabrication, thermal drawing can be applied to hybrid materials systems under the condition of the components having similar glass transition and/or melting temperatures [28, 29]. This may allow for basic studies of material-tissue interfaces for nerve regeneration as well as enable incorporation of additional functional features for future neuroprosthetic approaches. For example, alternative materials platforms may enable to address the observed lack of scalability of neurite outgrowth from 5 mm to 10 mm long fiber scaffolds (Fig. 4). We hypothesize that the proportional decrease in neurite growth rate into longer fibers is a result of limited nutrient exchange through the lumen of the longer scaffolds. This claim is supported by the observed increase in neurite outgrowth within larger grooved scaffolds (Fig. 4C, D). Notably the neurite outgrowth on the surface and the edges of fiber scaffolds is extensive and similar for rectangular and round external geometries (Table 3).

Tensile loading of injured peripheral nerve influences tissue repair [49] and should be considered in guidance channel design. Native peripheral nerve tissue is highly viscoelastic, capable of sustaining large deformations (~8% elongation) without damage to tissue, changes in conduction, or blood flow [50]. While the complex, hierarchical architecture of neural and connective tissue *in vivo* yields variability of bulk mechanical properties across peripheral nerve locations and species [51], DRG neurites exhibit a maximal outgrowth on substrates with a stiffness on the order of single kPa [52]. We

anticipate that matching the mechanical properties of materials constituting fiber-based neural scaffolds with those of nerve tissue will potentially improve biocompatibility and neurite growth [53] in future studies.

While microchannel scaffolds for separating regenerating axons were recently demonstrated *in vivo;* functional interrogation of the tissue infiltrating these neural scaffolds remains elusive [14]. Since thermal drawing was previously applied to integrate optical waveguides, electrodes, and microfluidic channels into neural fiber probes [29, 30], it may enable future incorporation of electrical [43, 54] or optical stimulation [32] means for accelerated nerve regeneration without sacrificing the valuable regenerative space.

5. Conclusions

With a high yield, fine control over microscale features, and compatibility with a wide range of materials, the thermal drawing process presents a promising tool for neural tissue engineering and its clinical applications in nerve repair. Taking advantage of the drawing process, we produced a diverse array of fiber-scaffolds that, for the first time, allowed for detailed investigation of the role of scaffold geometry and dimensions in neurite growth. Fiber scaffolds with rectangular and grooved channels strongly influence Schwann cell migration, as manifested in nuclear alignment and elongation. The latter were correlated with neurite orientation, and enhanced neurite growth through the channel. This work indicates that matching the dimensions of nerve guidance channels to those of individual fascicles may allow for accelerated nerve repair.

Acknowledgments:

This work was supported in part by the Charles Stark Draper Laboratory University Research and Development Grant, the MIT MRSEC through the MRSEC Program of the National Science Foundation (NSF) under awards DMR-0819762 and DMR-1419807, the NSF CAREER Award (CBET-1253890), and the National Institute for Neurological Disorders and Stroke (R01 NS086804-01A1). R.A.K. is a recipient of the translational fellowship from the Research Laboratory of Electronics. S.P. is a recipient of the Samsung Scholarship. The authors are grateful to P. Kasili and T. Paul for initial help with the experimental design.

References:

[1] Noble J, Munro CA, Prasad VS, Midha R. Analysis of upper and lower extremity peripheral nerve injuries in a population of patients with multiple injuries. J Trauma. 1998;45:116-22.
[2] Schmidt CE, Leach JB. Neural tissue engineering: strategies for repair and regeneration. Annu Rev Biomed Eng. 2003;5:293-347.
[3] Chen ZL, Yu WM, Strickland S. Peripheral regeneration. Annu Rev Neurosci. 2007;30:209-33.
[4] Lee SK, Wolfe SW. Peripheral nerve injury and repair. J Am Acad Orthop Surg. 2000;8:243-52.
[5] Portincasa A, Gozzo G, Parisi D, Annacontini L, Campanale A, Basso G, et al. Microsurgical treatment of injury to peripheral nerves in upper and lower limbs: a critical review of the last 8 years. Microsurgery. 2007;27:455-62.
[6] Pfister BJ, Gordon T, Loverde JR, Kochar AS, Mackinnon SE, Cullen DK. Biomedical engineering strategies for peripheral nerve repair: surgical applications, state of the art, and future challenges. Crit Rev Biomed Eng. 2011;39:81-124.
[7] Hu J, Zhu QT, Liu XL, Xu YB, Zhu JK. Repair of extended peripheral nerve lesions in rhesus monkeys using acellular allogenic nerve grafts implanted with autologous mesenchymal stem cells. Exp Neurol. 2007;204:658-66.
[8] Robinson LR. Traumatic injury to peripheral nerves. Muscle Nerve. 2000;23:863-73.
[9] Carriel V, Alaminos M, Garzon I, Campos A, Cornelissen M. Tissue engineering of the peripheral nervous system. Expert review of neurotherapeutics. 2014;14:301-18.
[10] Hoffman-Kim D, Mitchel JA, Bellamkonda RV. Topography, cell response, and nerve regeneration. Annu Rev Biomed Eng. 2010;12:203-31.
[11] Pateman CJ, Harding AJ, Glen A, Taylor CS, Christmas CR, Robinson PP, et al. Nerve guides manufactured from photocurable polymers to aid peripheral nerve repair. Biomaterials. 2015;49:77-89.
[12] Mobasseri A, Faroni A, Minogue BM, Downes S, Terenghi G, Reid AJ. Polymer scaffolds with preferential parallel grooves enhance nerve regeneration. Tissue engineering Part A. 2015;21:1152-62.
[13] Bell JH, Haycock JW. Next generation nerve guides: materials, fabrication, growth factors, and cell delivery. Tissue Eng Part B Rev. 2012;18:116-28.
[14] Stoyanova, II, van Wezel RJ, Rutten WL. In vivo testing of a 3D bifurcating microchannel scaffold inducing separation of regenerating axon bundles in peripheral nerves. Journal of neural engineering. 2013;10:066018.
[15] Pawar K, Mueller R, Caioni M, Prang P, Bogdahn U, Kunz W, et al. Increasing capillary diameter and the incorporation of gelatin enhance axon outgrowth in alginate-based anisotropic hydrogels. Acta Biomater. 2011;7:2826-34.
[16] Laquerriere A, Yun J, Tiollier J, Hemet J, Tadie M. Experimental evaluation of bilayered human collagen as a dural substitute. J Neurosurg. 1993;78:487-91.

[17] Yao L, de Ruiter GC, Wang H, Knight AM, Spinner RJ, Yaszemski MJ, et al. Controlling dispersion of axonal regeneration using a multichannel collagen nerve conduit. Biomaterials. 2010;31:5789-97.
[18] Ikeda M, Uemura T, Takamatsu K, Okada M, Kazuki K, Tabata Y, et al. Acceleration of peripheral nerve regeneration using nerve conduits in combination with induced pluripotent stem cell technology and a basic fibroblast growth factor drug delivery system. Journal of biomedical materials research Part A. 2014;102:1370-8.
[19] Baiguera S, Del Gaudio C, Lucatelli E, Kuevda E, Boieri M, Mazzanti B, et al. Electrospun gelatin scaffolds incorporating rat decellularized brain extracellular matrix for neural tissue engineering. Biomaterials. 2014;35:1205-14.
[20] Yang XN, Jin YQ, Bi H, Wei W, Cheng J, Liu ZY, et al. Peripheral nerve repair with epimysium conduit. Biomaterials. 2013;34:5606-16.
[21] Koppes AN, Seggio AM, Thompson DM. Neurite outgrowth is significantly increased by the simultaneous presentation of Schwann cells and moderate exogenous electric fields. Journal of neural engineering. 2011;8:046023.
[22] Al-Majed AA, Neumann CM, Brushart TM, Gordon T. Brief electrical stimulation promotes the speed and accuracy of motor axonal regeneration. J Neurosci. 2000;20:2602-8.
[23] Spivey EC, Khaing ZZ, Shear JB, Schmidt CE. The fundamental role of subcellular topography in peripheral nerve repair therapies. Biomaterials. 2012;33:4264-76.
[24] Richardson JA, Rementer CW, Bruder JM, Hoffman-Kim D. Guidance of dorsal root ganglion neurites and Schwann cells by isolated Schwann cell topography on poly(dimethyl siloxane) conduits and films. J Neural Eng. 2011;8:046015.
[25] Chua JS, Chng CP, Moe AA, Tann JY, Goh EL, Chiam KH, et al. Extending neurites sense the depth of the underlying topography during neuronal differentiation and contact guidance. Biomaterials. 2014;35:7750-61.
[26] Daly W, Yao L, Zeugolis D, Windebank A, Pandit A. A biomaterials approach to peripheral nerve regeneration: bridging the peripheral nerve gap and enhancing functional recovery. J R Soc Interface. 2012;9:202-21.
[27] Yaman M, Khudiyev T, Ozgur E, Kanik M, Aktas O, Ozgur EO, et al. Arrays of indefinitely long uniform nanowires and nanotubes. Nat Mater. 2011;10:494-501.
[28] Abouraddy AF, Bayindir M, Benoit G, Hart SD, Kuriki K, Orf N, et al. Towards multimaterial multifunctional fibres that see, hear, sense and communicate. Nat Mater. 2007;6:336-47.
[29] Canales A, Jia X, Froriep UP, Koppes RA, Tringides CM, Selvidge J, et al. Multifunctional fibers for simultaneous optical, electrical and chemical interrogation of neural circuits in vivo. Nat Biotechnol. 2015;33:277-84.
[30] Lu C, Froriep UP, Koppes RA, Canales A, Caggiano V, Selvidge J, et al. Polymer Fiber Probes Enable Optical Control of Spinal Cord and Muscle Function In Vivo. Adv Funct Mater. 2014;24:6594-600.
[31] Kozai TD, Langhals NB, Patel PR, Deng X, Zhang H, Smith KL, et al. Ultrasmall implantable composite microelectrodes with bioactive surfaces for chronic neural interfaces. Nat Mater. 2012;11:1065-73.
[32] Park S, Koppes RA, Froriep UP, Jia X, Achyuta AK, McLaughlin BL, et al. Optogenetic control of nerve growth. Sci Rep. 2015;5:9669.

[33] Schulz C, von Rusten-Lange M, Kruger A, Lendlein A, Jung F. Adherence and shear-resistance of primary human endothelial cells on smooth poly(ether imide) films. Clin Hemorheol Microcirc. 2014;57:147-58.
[34] Seifert B, Mihanetzis G, Groth T, Albrecht W, Richau K, Missirlis Y, et al. Polyetherimide: a new membrane-forming polymer for biomedical applications. Artif Organs. 2002;26:189-99.
[35] Zuidema JM, Hyzinski-Garcia MC, Van Vlasselaer K, Zaccor NW, Plopper GE, Mongin AA, et al. Enhanced GLT-1 mediated glutamate uptake and migration of primary astrocytes directed by fibronectin-coated electrospun poly-L-lactic acid fibers. Biomaterials. 2014;35:1439-49.
[36] Xie J, Liu W, MacEwan MR, Bridgman PC, Xia Y. Neurite outgrowth on electrospun nanofibers with uniaxial alignment: the effects of fiber density, surface coating, and supporting substrate. ACS nano. 2014;8:1878-85.
[37] Hsu SH, Ni HC. Fabrication of the microgrooved/microporous polylactide substrates as peripheral nerve conduits and in vivo evaluation. Tissue engineering Part A. 2009;15:1381-90.
[38] Koppes AN, Zaccor NW, Rivet CJ, Williams LA, Piselli JM, Gilbert RJ, et al. Neurite outgrowth on electrospun PLLA fibers is enhanced by exogenous electrical stimulation. Journal of neural engineering. 2014;11:046002.
[39] Panseri S, Cunha C, Lowery J, Del Carro U, Taraballi F, Amadio S, et al. Electrospun micro- and nanofiber tubes for functional nervous regeneration in sciatic nerve transections. BMC Biotechnol. 2008;8:39.
[40] Huang C, Ouyang Y, Niu H, He N, Ke Q, Jin X, et al. Nerve guidance conduits from aligned nanofibers: improvement of nerve regeneration through longitudinal nanogrooves on a fiber surface. ACS Appl Mater Interfaces. 2015;7:7189-96.
[41] Daud MF, Pawar KC, Claeyssens F, Ryan AJ, Haycock JW. An aligned 3D neuronal-glial co-culture model for peripheral nerve studies. Biomaterials. 2012;33:5901-13.
[42] Prinz C, Hallstrom W, Martensson T, Samuelson L, Montelius L, Kanje M. Axonal guidance on patterned free-standing nanowire surfaces. Nanotechnology. 2008;19:345101.
[43] Koppes AN, Nordberg AL, Paolillo GM, Goodsell NM, Darwish HA, Zhang L, et al. Electrical stimulation of schwann cells promotes sustained increases in neurite outgrowth. Tissue engineering Part A. 2014;20:494-506.
[44] Thompson DM, Buettner HM. Oriented Schwann cell monolayers for directed neurite outgrowth. Ann Biomed Eng. 2004;32:1120-30.
[45] Guenard V, Kleitman N, Morrissey TK, Bunge RP, Aebischer P. Syngeneic Schwann cells derived from adult nerves seeded in semipermeable guidance channels enhance peripheral nerve regeneration. J Neurosci. 1992;12:3310-20.
[46] Sheets K, Wunsch S, Ng C, Nain AS. Shape-dependent cell migration and focal adhesion organization on suspended and aligned nanofiber scaffolds. Acta Biomater. 2013;9:7169-77.
[47] Mitchel JA, Hoffman-Kim D. Cellular scale anisotropic topography guides Schwann cell motility. PLoS One. 2011;6:e24316.

[48] Wang HB, Mullins ME, Cregg JM, McCarthy CW, Gilbert RJ. Varying the diameter of aligned electrospun fibers alters neurite outgrowth and Schwann cell migration. Acta Biomater. 2010;6:2970-8.
[49] Piao CD, Yang K, Li P, Luo M. Autologous nerve graft repair of different degrees of sciatic nerve defect: stress and displacement at the anastomosis in a three-dimensional fnite element simulation model. Neural Regen Res. 2015;10:804-7.
[50] Driscoll PJ, Glasby MA, Lawson GM. An in vivo study of peripheral nerves in continuity: biomechanical and physiological responses to elongation. J Orthop Res. 2002;20:370-5.
[51] Georgeu GA, Walbeehm ET, Tillett R, Afoke A, Brown RA, Phillips JB. Investigating the mechanical shear-plane between core and sheath elements of peripheral nerves. Cell Tissue Res. 2005;320:229-34.
[52] Koch D, Rosoff WJ, Jiang J, Geller HM, Urbach JS. Strength in the periphery: growth cone biomechanics and substrate rigidity response in peripheral and central nervous system neurons. Biophys J. 2012;102:452-60.
[53] Piao C, Li P, Liu G, Yang K. Viscoelasticity of repaired sciatic nerve by poly(lactic-co-glycolic acid) tubes. Neural Regen Res. 2013;8:3131-8.
[54] Balint R, Cassidy NJ, Cartmell SH. Electrical stimulation: a novel tool for tissue engineering. Tissue engineering Part B, Reviews. 2013;19:48-57.

Thermally Drawn Fibers as Nerve Guidance Scaffolds

Authors:
Ryan A. Koppes[12], Seongjun Park[1,3], Tiffany Hood[4], Xiaoting Jia[1], Negin Abdolrahim Poorheravi[5], Anilkumar Harapanahalli Achyuta[6], Yoel Fink[1,7], Polina Anikeeva[1,7]

Affiliations:
[1]Research Laboratory of Electronics, Massachusetts Institute of Technology, Cambridge, Massachusetts 02139
[2]Department of Chemical Engineering, Northeastern University, Boston, Massachusetts 02115
[3]Department of Electrical Engineering and Computer Science, Massachusetts Institute of Technology, Cambridge, Massachusetts 02139
[4]Department of Bioengineering, Massachusetts Institute of Technology, Cambridge, Massachusetts 02139
[5]Department of Mechanical Engineering, Massachusetts Institute of Technology, Cambridge, Massachusetts 02139, United States
[6]Draper Laboratory**,** 555 Technology Square, Cambridge, Massachusetts 02139
[7]Department of Materials Science and Engineering, Massachusetts Institute of Technology, Cambridge, Massachusetts 02139

Supplementary Information

Bending Stiffness:

Mechanical properties for PEI fiber NGCs were found as outlined by Kozai et al. The axial spring constant for round and rectangular fibers was calculated as:

$$k = \frac{AE}{L} \quad (1)$$

where *A* is the cross-sectional area, *E* is the elastic moduls of PEI (104.8 MPa), and L is the length of the fiber (10 mm).

$$k = \frac{3EI}{L^3} \quad (2)$$

where *I* is defined as:

$$I = \frac{\pi({d_o}^4 - {d_i}^4)}{64} \quad (3)$$

for a hollow cylinder, where d_o is the outer and d_i is the inner diameter. For a hollow rectangular beam, *I* is defined as:

$$I = \frac{W_o {H_o}^3}{12} - \frac{W_i {H_i}^3}{12} \quad (4)$$

where the outer dimensions are defined by W_o and H_o and the hollow core dimensions are W_i and H_i.

Three Dimensional Confocal Reconstructions:

Image stacks were imported into ImageJ, opened in the Volume Viewer plugin, and snapshots of 3D volumes were acquired.

Supplementary Figures:

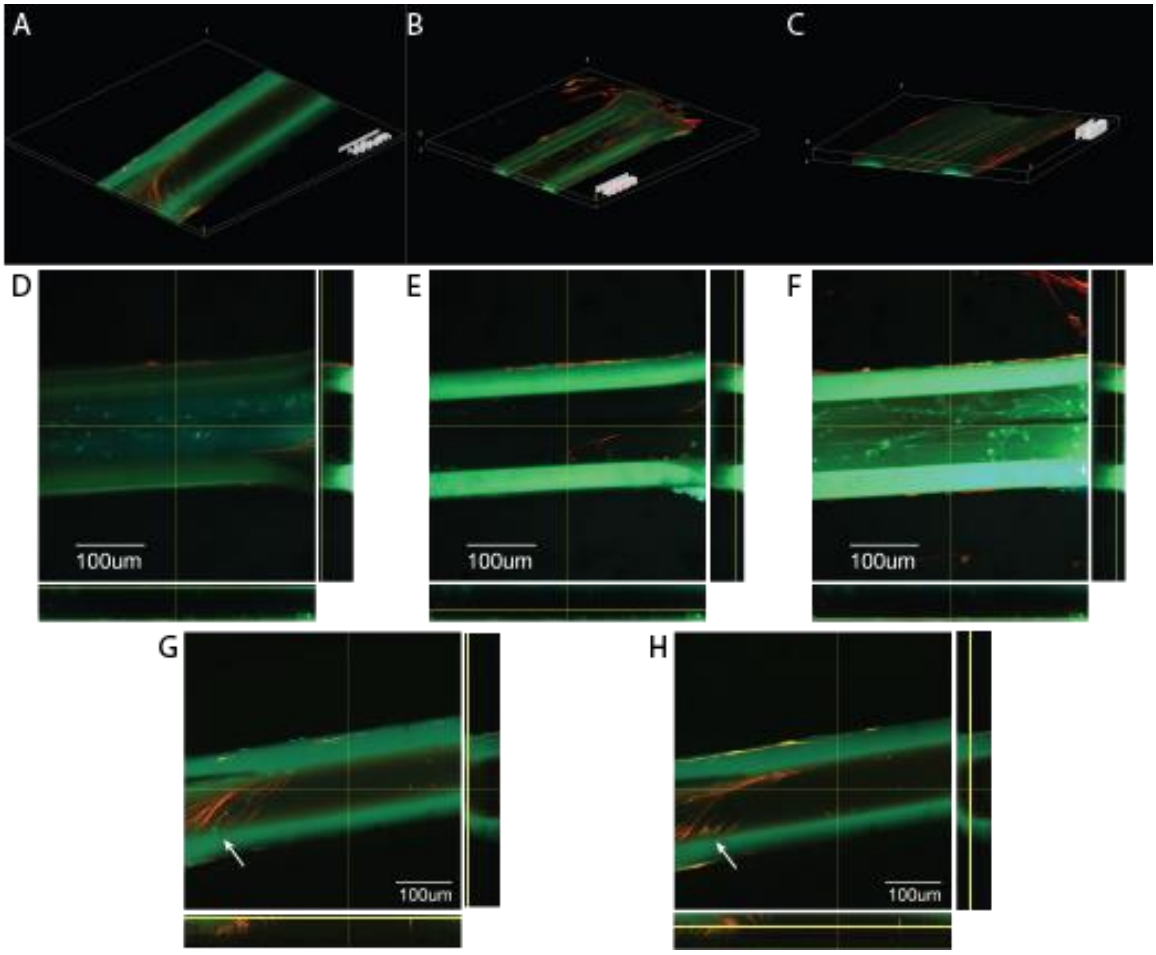

Supplementary Figure 1. Three dimensional representations of confocal z-stack images. Fibers were fixed and stained for cell nuclei (DAPI, blue), F-actin (phallodin, green), Schwann cells (s-100, orange), and neurites (neurofilament, red). Volume representations of outgrowth into (A) round, (B) square, and (C) grooved fiber scaffolds. (D-F) Individual XY-planes and orthogonal views (XZ & YZ) for three different Z-depths within a square fiber demonstrate how neurites grow on all surfaces of the inner channel as well as the spatial differences of Schwann cells, location of actin, and neurites. (G, H)

Individual XY-planes and orthogonal views (XZ & YZ) for two different Z-depths within a cylindrical fiber demonstrate how the structure of neurites and Schwann cells as well as their corresponding nuclei (i.e. white arrows designate single Schwann Cell and nucleus) is three-dimensional and cannot be accurately represented by a single slice.

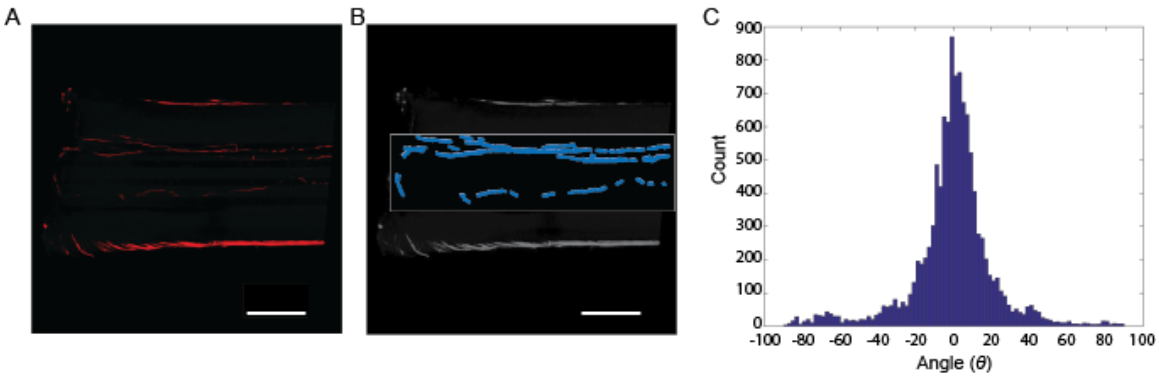

Supplementary Figure 2. Neurite orientation analysis. (A) Representative image of neurite ingrowth in to a grooved channel. (B) Short segments of neurites within the channel are fitted with blue orthogonal lines. For each segment, the major angle with respect to the fiber axis was found. (C) A histogram of major angles for the image in (A). (scale bars = 100 μm).

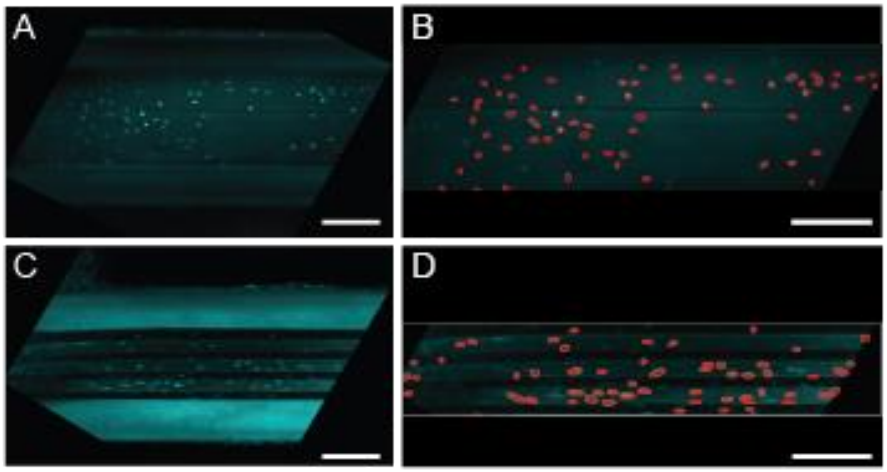

Supplementary Figure 3. Representative images of nuclei within (A, B) rectangular and (C, D) grooved fiber scaffolds (scale bars = 100 μm). (B, D) Nuclei are outlined by fitted red ellipsoids. Ellipsoid fits were used to calculate the major and minor radii as well as the angle of the major axis in reference to the direction of the fiber channel.

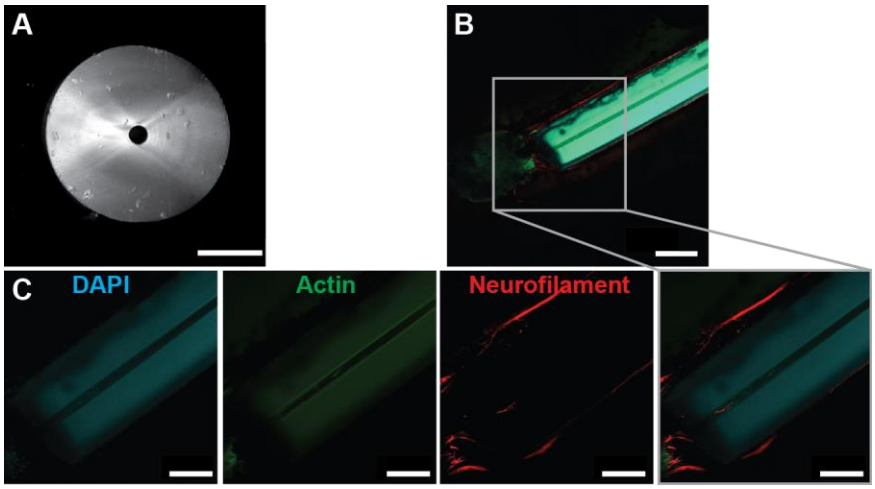

Supplementary Figure 4. Neurite outgrowth is limited in channels narrower than 50 μm. (A) To test round channels of geometries much lower than 50 μm, an additional PEI fiber was drawn (scale bar = 100 μm). (B) Cell migration and neurite outgrowth was observed on the external surface of the fibers, but very limited within the lumen of the scaffold (scale bar = 200 μm). (C) Closer inspection demonstrates cell infiltration (blue nuclie; DAPI) and neurite growth (red neurites; neurofilament) into a 30 μm channel (scale bars = 200 μm).

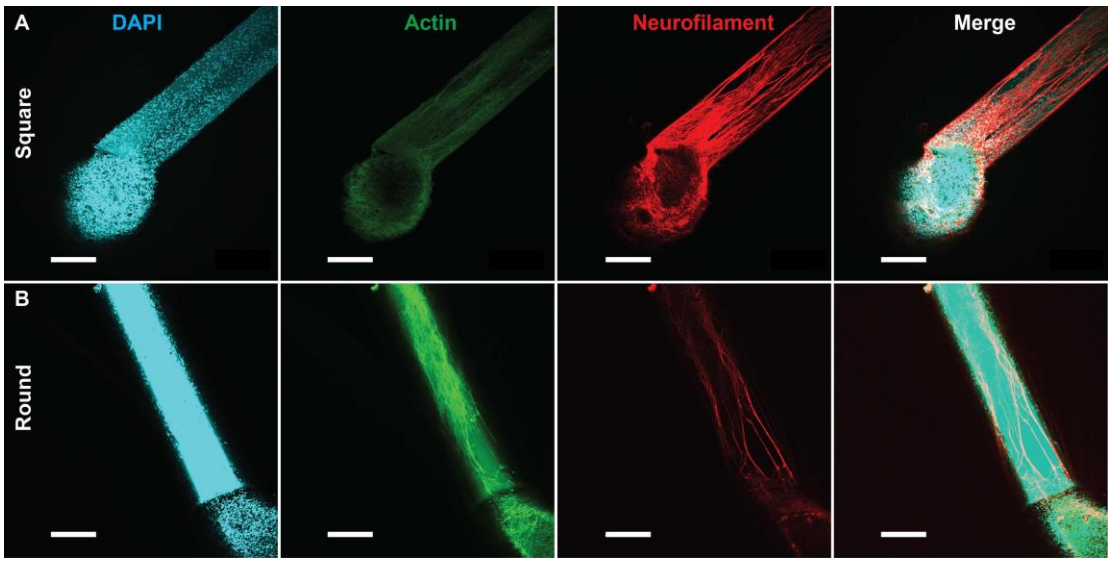

Supplementary Figure 5. DRG outgrowth onto the surface and edges of fiber NGCs after fourteen days of growth. Fibers were fixed and stained for cell nuclei (DAPI, blue), F-actin (phallodin, green), and neurites (neurofilament, red). Outgrowth onto (A) round and (B) square NGCs. Scale bars=100 μm.

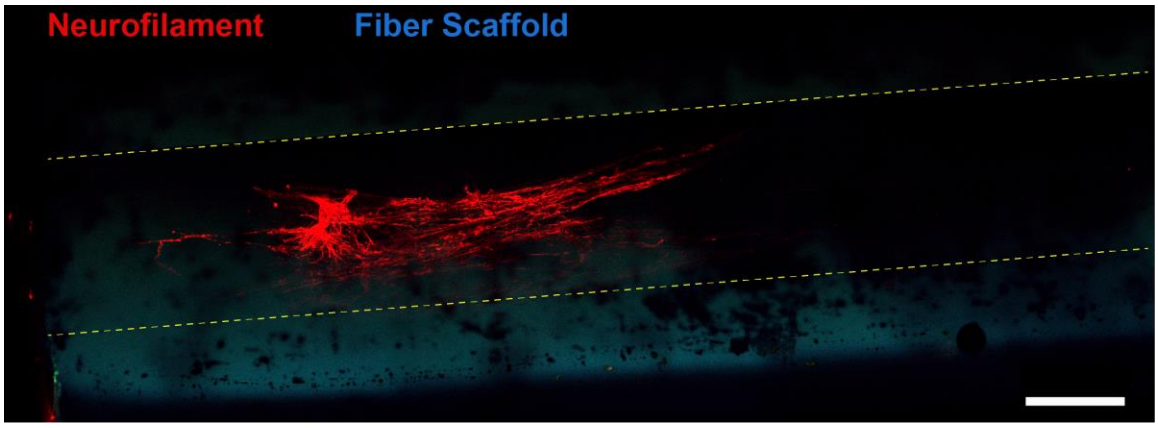

Supplementary Figure 6. DRG growth within the channel of a large rectangular fiber scaffold without the addition of Matrigel® after 1 week of growth. Scale bar = 300 μm.